THE JOURNAL OF PHYSICAL CHEMISTRY A

Article

pubs.acs.org/JPCA

Temperature Dependence in the Terahertz Spectrum of Nicotinamide: Anharmonicity and Hydrogen-Bonded Network

Masae Takahashi,*[,†,‡] Nubuyuki Okamura,[†,‡] Xinyi Fan,[†] Hitoshi Shirakawa,[†] and Hiroaki Minamide[‡]

[†]Graduate School of Agricultural Science, Tohoku University, Sendai 980-0845, Japan

[‡]RIKEN Advanced Science Institute, Sendai 980-0845, Japan

ABSTRACT: We have investigated the terahertz-spectral property of nicotinamide focusing on the temperature dependence in the range of 14−300 K. We observed that almost all peaks in the terahertz spectrum of the nicotinamide crystal showed a remarkable shift with temperature, whereas the lowest-frequency peak at 34.8 cm^{-1} showed a negligible shift with temperature. By analyzing the terahertz spectrum with the dispersion-corrected density functional theory calculations, we found that the difference in the temperature dependence of the peak shift is well understood in terms of the presence/absence of stretching vibration of the intermolecular hydrogen bond in the mode and the change of cell parameters. The anharmonicity in the dissociation potential energy of very weak intermolecular hydrogen bonding causes the remarkable peak shift with temperature in the terahertz spectrum of nicotinamide. This finding suggests that the assignment and identification of peaks in the terahertz spectrum are systematically enabled by temperature-dependent measurements.

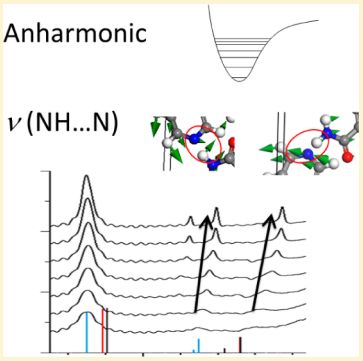

1. INTRODUCTION

Terahertz (THz) spectroscopy is a powerful tool for detecting weak noncovalent intermolecular bonds such as hydrogen bonds and van der Waals (vdW) forces,[1−3] both of which are common and essential bonds between molecules, irrespective of the species of molecules. Biopolymers, such as proteins, nucleic acids, and sugars, utilize the intermolecular motion of THz vibrations that are excited with a mild thermal energy at room temperature, which causes the conformational change to achieve various novel functions that are characteristic of each molecule. Because of the recent remarkable progress in dispersion-corrected first-principles (or density functional theory (DFT)) calculations, peak assignment in a THz spectrum has become considerably reliable.[4−16] Combined with these theoretical calculations, THz spectroscopy is now able to provide precise information on various thermal properties of intermolecular vibrations in complicated molecular systems including biological and medical systems.

It has been reported that the peak position in a THz spectrum shows a remarkable shift with temperature.[13−18] Although the origin is presumably the anharmonicity of the potential energy curve and/or the temperature-dependent change of the volume, the details have not been well understood. In particular, THz vibration, which is a low vibrational excitation, curiously exhibits substantial temperature dependence, although the effect of anharmonicity in the potential energy on the vibrational absorption frequency is expected to be prominent in the regions at high vibrational excitations where the parabolic approximation is poor. To gain insight into the nature of intermolecular vibrations that are relevant to the function of molecules, it is important to elucidate the anomalous temperature dependence of THz vibrations.

Vitamins are classified into two different categories, water-soluble and fat-soluble,[19] and nicotinamide (pyridine-3-carboxamide) is a water-soluble vitamin. Vitamins are an essential factor for the maintenance of metabolism. The functions of vitamins have been extensively elucidated, but recent studies indicate that a pharmacological dose of vitamins has novel properties for the prevention and curing of diseases.[20,21] Each vitamin has a characteristic structure and molar mass, but almost all vitamins have a common part, which mimics DNA or amino acids. The THz spectrum of nicotinamide was first reported in 2009,[22] but the relationship of the spectrum with the water-soluble property and resultant vitamin function has not been well elucidated. Nicotinamide molecules are connected to each other via a hydrogen-bonded network in crystals, whereas the hydrogen bonds between nicotinamide molecules are replaced with those between the nicotinamide and water molecules when nicotinamide is dissolved in water. We have investigated several water-addition reactions[23−26] and found that the reaction starts with the formation of an initial complex via intermolecular hydrogen bonding. It is argued with ionic liquids[27−29] that stronger intermolecular hydrogen bonds lead to larger wavenumbers and stronger intensities of the corresponding hydrogen bond stretching vibrations between molecules. However, the temperature dependence of the hydrogen bond stretching vibrations between molecules has not been unraveled.

Received: November 3, 2016
Revised: February 20, 2017
Published: March 20, 2017

DOI: 10.1021/acs.jpca.6b11049
J. Phys. Chem. A 2017, 121, 2558−2564

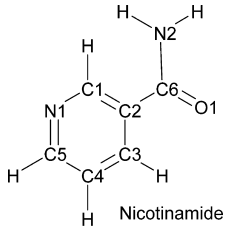

In this paper, we report a THz spectroscopic study on a water-soluble vitamin, nicotinamide. The mass is sufficiently small to distinguish the intermolecular and intramolecular vibrations very well. This condition is a large advantage in observing the detailed temperature dependence of the THz spectrum. We observed here anomalous temperature-dependent behavior in the THz spectrum of nicotinamide, which shows sharp contrast to a well-known temperature-dependent frequency shift.[13−18] We have analyzed the THz spectrum with the dispersion-corrected DFT calculations to investigate the origin of the anomalous temperature dependence.

2. EXPERIMENT

The THz spectrum was measured with a Bomem DA-8 Fourier-transform infrared spectrometer, which was equipped with a 4 K-silicon bolometer. A cryostat (OPTISTAT-CF; Oxford Instruments, plc.) was used for low-temperature measurements.

Nicotinamide was purchased from Wako Pure Chemical Industries and used without further purification. Nicotinamide was mixed with a powdered polyethylene (PE) matrix at 3.5% by mass to ensure that the measurements were made within an optimal absorption range. Because PE is nearly transparent in the far-infrared region, it is a suitable filling material for spectroscopic applications. The sample mixture was pressed at 3 tons into a pellet with a diameter of 13 mm and a thickness of approximately 1 mm. To obtain a clear spectrum in the range of 25−165 cm^{-1}, we measured a 14% thicker pellet. PE was pressed into a pellet of equal mass to use as a blank reference. The ratio of the data sets of the sample and blank resulted in a THz spectrum in the range of 25−210 cm^{-1} with a spectral resolution of 0.5 cm^{-1}. The experimental frequencies and full width at half-maximum (fwhm) of the peaks in Table 1 were evaluated by fitting the spectrum with a Lorentz function.

3. COMPUTATIONAL DETAILS

Dispersion-corrected DFT calculations of the crystal were performed with the CATEP code (ver.8.0).[30] Total-energy calculation was based on the plane-wave DFT method within the generalized gradient approximation. Perdew−Burke−Ernzerhof (PBE) exchange−correlation functionals[31,32] were used as implemented in the CASTEP code.[30] The PBE functional was selected because it consistently produces a high-quality simulation of the solid-state structure and a THz spectrum.[33] The norm-conserving pseudopotential was used to describe the electron−ion interaction. The Tkatchenko−Scheffler (TS) method[34] was used for dispersion correction. The valence electron wave function was expanded in terms of the plane-wave basis set to a 1200 eV kinetic energy cutoff. The electronic minimization was converged to less than 10^{-13} eV/atom using a conjugate gradient scheme (the force on each atom was reduced to below 1×10^{-5} eV/Å for full optimizations and 2×10^{-3} eV/Å for the fixed-cell calculation). Brillouin zone integration was performed using the Monkhorst−Pack method with a k-point mesh with an interval of 0.07 $Å^{-1}$. The total energy of the system converged to less than 10^{-4} eV/atom in terms of k-point sampling, total energy convergence, and so forth. Vibrational frequencies of the normal modes were calculated at the Γ-point within the harmonic approximation by numerically differentiating the analytical gradient of the potential energy with respect to the atomic position. The amplitude of displacements in the frequency calculation was set at 0.005 Å, unless otherwise noted. We have confirmed that there are three phonon modes with zero frequency, which validates the present vibrational frequency calculations because the total energy should be invariant under translation of the entire crystal. The mode descriptions and assignments were performed by visually inspecting the eigenvector atomic displacements for each normal mode.

Table 1. Terahertz Vibrations of Nicotinamide

	expt[a]		calcd[b]			
peak no.	freq[d] /cm^{-1}	fwhm[e] /cm^{-1}	freq[d] /cm^{-1}	int.[f] /km mol^{-1}	Δ[g] /cm^{-1}	description[c]
	19.43[h]	–	16.66 (−2.77)	1.4		T_a
1	34.84	2.96	39.24 (4.40)	15.4	4.35	R_c
2	62.57	1.04	71.99 (9.42)	1.6	8.40	R_b
3	69.47	1.10	76.05 (6.58)	5.4	11.08	$R_a + \nu$ (N2H···N1)
4	87.08	1.04	100.33 (13.25)	3.2	5.13	$T_b + \nu$ (N2H···N1)
5	97.47	–	100.61 (3.14)	1.4	4.90	$R_c + \nu$ (C1H···O1)
6	106.13	4.33	112.27 (6.14)	27.7	10.95	$R_b + \nu$ (C1H···O1)
7	115.85	1.92	121.05 (5.20)	2.1	9.70	τ (−$CONH_2$)
8	128.24	9.85	137.06 (8.82)	34.6	7.62	τ (−$CONH_2$)
9	192.50	8.04	195.40 (2.90)	49.4	9.76	γ
			197.64	9.5	7.59	γ

[a]Experimental results on peaks 1−9 at 14 K in Figure 1. [b]Calculated frequencies at the full optimization of the P_1 cell (red bars in Figure 1) with an intensity greater than 1 km mol^{-1}. [c]R_j: Intermolecular or lattice rotation about the j axis; T_j: intermolecular translation about the j axis; ν: stretching; τ: torsion; γ: out-of-plane bending. The crystalline axes are shown in Figure 3. [d]Frequency of peaks. The difference from the experimental value is given in parentheses. [e]Full width at half-maximum of the peak. [f]Intensity. [g]Difference of the calculated frequencies at the full optimization of the P_1 cell (red bars in Figure 1) from those at the fixed-cell optimization (blue bars in Figure 1). [h]Experimental result at 78 K from ref 35.

DOI: 10.1021/acs.jpca.6b11049
J. Phys. Chem. A 2017, 121, 2558−2564

4. RESULTS AND DISCUSSION

4.A. THz Spectra of Nicotinamide. Figure 1 shows the THz spectra of nicotinamide in the range of 25−210 cm^{-1}

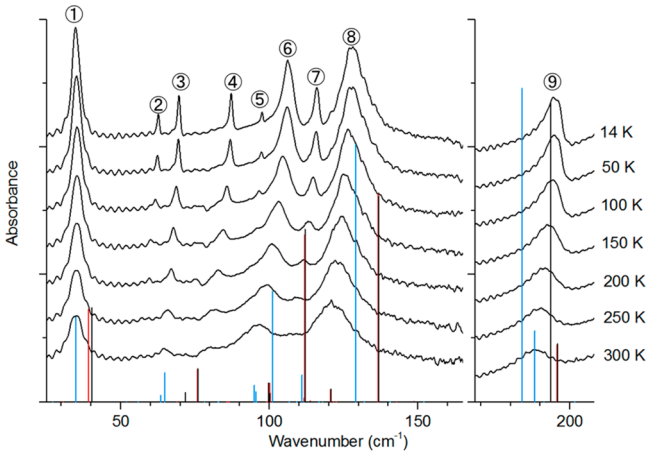

Figure 1. THz spectra of nicotinamide measured at various temperatures of 14−300 K. The observed peaks at 14 K are numbered from the low frequency. Solid bars indicate the calculated frequencies, and the height represents the relative intensity. Red: full optimization of the P_1 cell; black: full optimization of the $P_{21/c}$ cell; blue: optimization at the experimental unit cell.

measured at various temperatures of 14−300 K. We observe nine peaks at 14 K (peaks 1−9), and the number of peaks is reduced to seven at 300 K because of thermal broadening. The frequencies and fwhm's observed at 14 K are summarized in Table 1. Korter and co-workers reported the THz spectrum of nicotinamide in the wavenumber region of 10−90 cm^{-1}.[35] Their experimental result is essentially identical to ours in this low-frequency region and validates the present experimental results, which extend to the higher-frequency region over 210 cm^{-1}. Peak 1 at approximately 35 cm^{-1} in Figure 1 shows a negligible frequency shift with temperature, although the peak position in the THz spectrum usually shows a significant temperature-dependent shift.[13−18] In fact, the other eight peaks (peaks 2−9) at 14 K gradually shifted to lower frequencies with the increase of temperature.

4.B. Solid-State Calculations of Nicotinamide. To analyze the observed THz spectra, we performed DFT calculations on a nicotinamide crystal with the pairwise TS method[34] for dispersion correction. No scaling was applied for the calculated frequency values. The frequency of each normal mode was calculated within the harmonic approximation at the optimized geometry. The geometries were optimized using three different ways: (i) full optimization with no symmetry (P_1), where both cell parameters and atomic coordinates were optimized without maintaining the fractional coordinate during the lattice change (red bars in Figure 1); (ii) full optimization as (i) but under symmetry constraint ($P_{21/c}$) (black bars); (iii) optimization in the fixed cell for the room-temperature (295 K) crystallographic data[36] (blue bars). The full geometry optimization of (i) and (ii) began with X-ray crystallographic data at 150 K.[36] The calculated total energy hardly decreased, even when the symmetry was lowered from $P_{21/c}$ (−7983.34886 eV) to P_1 (−7983.34890 eV). The optimized cell parameters are slightly different from the experimental values at 150 K[36] by 1% for both the P_1 and $P_{21/c}$ cells (calculated cell parameters are a = 3.856 Å, b = 15.662 Å, c = 9.298 Å, α = 90.00°, β = 97.16°, and γ = 90.00° for both the P_1 and $P_{21/c}$ cells; experimental cell parameters at 150 K[36] are a = 3.877 Å, b = 15.60 Å, c = 9.375 Å, α = 90.00°, β = 98.45°, and γ = 90.00°). Under the rough tolerance (0.001 Å), the optimized P_1 cell exhibited $P_{21/c}$ symmetry. The present set of optimized cell parameters for both the P_1 and $P_{21/c}$ unit cells is more consistent with the experimental data set than previous calculations[35] with the Grimme method[37] for dispersion correction. The difference in calculated THz frequencies between full optimizations at different crystal symmetries (the red and black bars in Figure 1) is pronounced in the low-frequency region below 50 cm^{-1}, which indicates that the THz spectrum at low frequency is notably sensitive to the crystal symmetry.

The calculated frequencies, intensity, and mode description without symmetry constraint (P_1) are listed in Table 1, together with the present experimental results at 14 K. We described and assigned the modes by visually inspecting the eigenvector atomic displacements for each normal mode. Because full optimization of geometry reproduces the crystal structure at absolute zero temperature, the frequency data calculated at the fully optimized geometry are adequate for comparison with the low-temperature THz spectrum. Table 1 shows that the calculated frequency and relative intensity of each mode are consistent with the experimental result at 14 K. An accuracy of 10 cm^{-1} or less, except peak 4 (T_b), is the same as that in our previous results on the weak hydrogen bond system.[14] Although the calculated translation and torsion modes, even if those contain no weak hydrogen-bond stretching, frequently give a large difference from experimental values relative to the other modes,[14] a difference of 13 cm^{-1} in peak 4 (T_b) is still large. The results in Table 1 show that the intramolecular mode has a larger fwhm, except for peak 7. The mode description was consistent between the two optimization methods, (i) without symmetry constraint (P_1 cell) and (ii) with symmetry constraint ($P_{21/c}$ cell), but the stretching mode of a weak hydrogen bond was enhanced in low-symmetry optimization (P_1 cell) compared to that in high-symmetry optimization ($P_{21/c}$ cell).

4.C. Origin of the Temperature-Dependent Feature of THz Peaks. Figure 2 shows the observed frequency shift as a

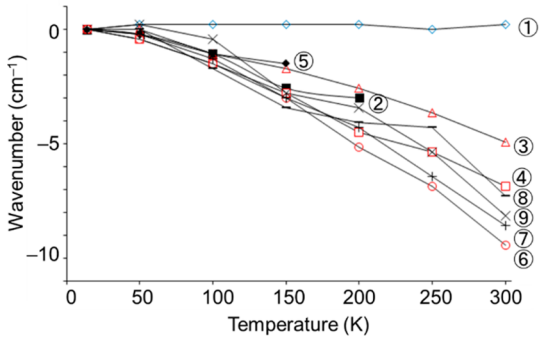

Figure 2. Frequency shift of THz peaks with temperature. Numbers 1−9 correspond to the peaks in Figure 1.

function of temperature for each peak. Peak 1 shows a negligible shift with temperature, whereas peaks 2−9 show a significant frequency shift of 5−10 cm^{-1} to lower frequencies with the increase of temperature from 14 to 300 K. The peak shift between 300 and 14 K is R_c (peak 1) ≪ R_a (peak 3) < T_b (peak 4) < τ (peaks 7 and 8), γ (peak 9) < R_b (peak 6). Experimentally, the cell parameters expand with heating from

DOI: 10.1021/acs.jpca.6b11049
J. Phys. Chem. A 2017, 121, 2558−2564

150 to 295 K[36] by 0.097 Å on the *a* axis, 0.04 Å on the *b* axis, and 0.055 Å on the *c* axis. Because the differences in the two axes other than the rotation axis affect the intermolecular rotation, the peak shift deduced from the volume expansion with temperature is $R_a \ll R_c < R_b$. The deduced peak shift on R_c and R_b ($R_c < R_b$) is consistent with experimentally observed peak sift (peak 1 < peak 6 in Figure 2). However, the small peak shift of peak 3 (R_a) deduced from volume expansion ($R_a \ll R_c < R_b$) is inconsistent with the observed shift of peak 3 (R_a) that is larger than the shift of peak 1 (R_c) (see Figure 2). A temperature-dependent shift of peak 3 would be caused by a different reason, such as the presence of anharmonicity in the potential energy curve.

The lattice constant of the unit cell will increase at finite temperatures, affecting the intermolecular interaction in the THz energy region. The cell parameters obtained by full optimization with the DFT calculation correspond to those at absolute zero temperature. As a model to represent the THz spectrum at 300 K, we have calculated the THz vibrations at the optimized geometry in the fixed cell for room-temperature (295 K) crystallographic data[36] (blue bars in Figure 1). First-principles molecular dynamics studies would be much better in some cases,[38−42] and we will perform them as future work. The fixed-cell calculation (blue bars) yields lower frequencies for all peaks 1−9 than the other two cases (red and black bars). The difference of calculated frequencies between the two different calculations, full optimization with no symmetry (P_1) (red bars in Figure 1) and optimization in the fixed cell for the room-temperature crystallographic data[36] (blue bars in Figure 1), is listed as Δ in Table 1. The intramolecular C−H and N−H distances do not change among full optimizations for the P_1 and $P_{21/c}$ unit cells and the fixed-cell optimization. On the other hand, the intermolecular (C)H···O and (N)H···N distances elongate in the fixed-cell calculation (r((C)H···O): 2.567 and 2.488 Å; r(N)H···N)): 2.003 Å; see Figure 3 for those

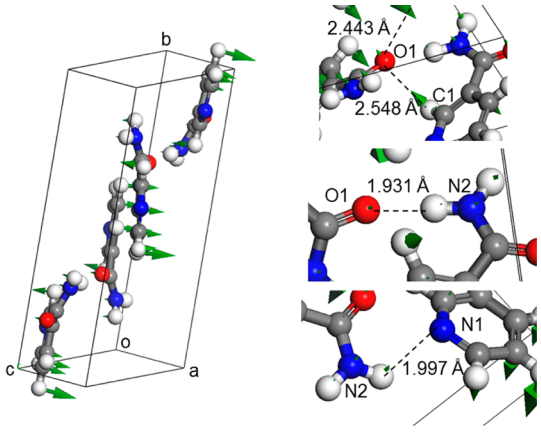

Figure 3. Calculated vibrational mode of peak 1. Green arrows indicate the displacement vectors. In the right panel, three types of intermolecular hydrogen bonds are shown with dashed lines, and the calculated bond lengths (P_1 cell) are given.

intermolecular distances of the fully optimized P_1 cell; those intermolecular distances of the $P_{21/c}$ cell are the same as those of the P_1 cell). The frequency values of respective modes change due to the elongating intermolecular distances and the resultant difference in packing effect. It is proved that the volume expansion with temperature is actually one origin of the frequency shift of THz vibrations.

The other possible origin of the temperature-dependent peak shift is the anharmonicity of the potential energy curve. We investigate the anharmonicity by increasing the amplitude of displacements in the frequency calculation (Table 2). When the

Table 2. Anharmonicity in THz Vibrations[a]

peak no.[b]	displacement/Å		
	0.005	0.010	0.015
1	39.24	39.60 (0.35)	40.98 (1.74)
2	71.99	71.32 (−0.68)	71.12 (−0.88)
3	76.05	74.85 (−1.19)	73.32 (−2.73)
4	100.33	99.66 (−0.68)	98.58 (−1.75)
5	100.61	100.55 (−0.06)	101.12 (0.51)
6	112.27	111.95 (−0.32)	111.88 (−0.38)
7	121.05	121.06 (0.01)	121.05 (0.00)
8	137.06	137.17 (0.11)	137.48 (0.42)
9	195.40	195.43 (0.03)	195.54 (0.14)

[a]Frequencies at the fully optimized geometry of the P_1 cell are given in cm^{-1} at the respective amplitude of displacement from 0.005 to 0.015 Å. The difference from the frequency at 0.005 Å of the displacement amplitude is given in parentheses. [b]Numbers 1−9 correspond to the peaks in Figure 1.

potential energy curve is anharmonic, the frequency changes with increasing amplitude of the displacements. No frequency shift guarantees the harmonic feature of the potential energy curve. As shown in Table 2, peaks 1 (R_c), 5 (R_c), 7 (τ), 8 (τ), and 9 (γ) give no frequency shift or a slight shift to higher frequency (zero or positive difference given in parentheses) with the increase in the displacement amplitude. On the other hand, peaks 2 (R_b), 3 (R_a), 4 (T_b), and 6 (R_b) show the shift to lower frequency (negative difference given in parentheses). The shift to higher frequency with the increase in the displacement amplitude means an effect of the intermolecular or interatomic repulsions, while that to lower frequency is ascribed to the anharmonic feature of the dissociation or double-minimum potential energies. The effect of the intermolecular or interatomic repulsions is enhanced in the lower vibrational frequencies probably due to the shallow potential energy curve. Because the shift of peak 1 to low frequency by volume expansion with the increase of temperature is compensated by the shift to high frequency by the effect of the intermolecular or interatomic repulsions, peak 1 would show a stationary feature with temperature. The negative frequency shift by the anharmonic feature of the potential energy curve (Table 2) is small in R_b (peaks 2 and 6) compared with that of R_a (peak 3) and T_b (peak 4). The rotation mode along the *b* axis (R_b) would have a double minimum with six-membered rings of two molecules in the plane at the maximum, while the translation T_b and rotation R_a modes do not have a double minimum. The large negative frequency shift of peaks 3 and 4 in Table 2 would be explained by the anharmonicity in the dissociation potential energy of a weak hydrogen bond.

Peaks 3−6 contain the stretching vibration of weak intermolecular hydrogen bonds (Table 1). The left panel of Figure 3 depicts the motion of peak 1 that does not contain the stretching vibration of any hydrogen bonds between molecules, while Figure 4 shows the motion of peaks 3−6 that involve the stretching vibration of intermolecular hydrogen bonds. Peak 1 is assigned to the out-of-plane R_c (intermolecular rotation about the *c* axis) vibration mode, and the out-of-plane motions without the stretching vibration of weak hydrogen bonds like

DOI: 10.1021/acs.jpca.6b11049
J. Phys. Chem. A 2017, 121, 2558−2564

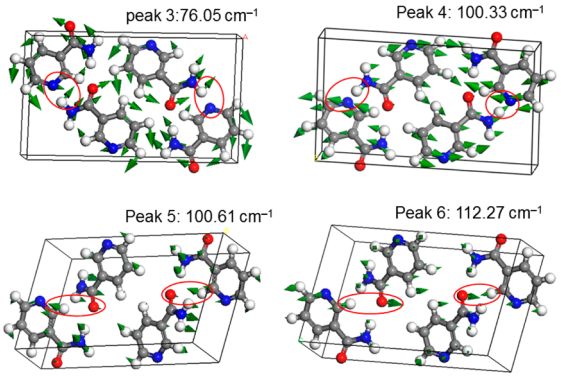

Figure 4. Calculated vibrational modes of peaks 3−6 with weak hydrogen-bond stretching vibrations between molecules. Green arrows indicate the displacement vectors. The stretching vibrations of the hydrogen bond are marked by red circles.

peak 1 (R_c) would promote the insertion of a water molecule between nicotinamide molecules. Solubility in water is an essential factor for nicotinamide to realize its vital function, and insertion of a water molecule would be the first step of the process. Nicotinamide in crystal form has three different hydrogen bonds among nicotinamide molecules: N2H···N1, N2H···O1, and C1H···O1 (the right panel of Figure 3); those are classified as "weak" hydrogen bonds.[43] The dissociation energy of a weak hydrogen bond is sufficiently small (0.4−4 kcal/mol),[44] and thus, the anharmonicity of the dissociation potential energy would affect the vibrational frequency in the THz energy region. The modes containing the N2H···N1 stretching (peaks 3 and 4) actually show a significant frequency shift that suggests the distinct anharmonicity affecting the THz vibrations (Table 2). On the other hand, the frequency shift of the modes containing the C1H···O1 stretching (peaks 5 and 6) is less remarkable (Table 2). It would be because two C1H···O1 bonds are formed at one O1 atom from opposite directions (see the right panel of Figure 3). The switching of the hydrogen bond from that between nicotinamide molecules to that between the nicotinamide and water would promote solvation into water via the stretching vibration of the weak hydrogen bond like peaks 3 and 4.

The calculated frequencies (cm^{-1}) of all modes containing intermolecular hydrogen-bond stretching in the P_1 cell are

ν(N2H···N1): 76.05 (R_a; 5.4 km/mol), 88.95 (R_a; 0.0 km/mol), 100.33 (T_b; 3.2 km/mol), 121.96 (R_a; 0.0 km/mol)

ν(N2H···O1): 148.94 (T_c; 0.0 km/mol), 149.17 (T_c; 0.0 km/mol)

ν(C1H···O1): 99.47 (T_a; 0.0 km/mol), 100.61 (R_c; 1.4 km/mol), 112.27 (R_b; 27.7 km/mol), 122.89 (R_a; 0.0 km/mol)

where the intermolecular mode and the intensity are indicated in parentheses. Because the N2H···O1 bond is nearly along the *c* axis, the stretching vibrations are involved in the intermolecular translation modes about the *c* axis (T_c). The C1H···O1 bond is mainly along the *a* axis but is tilted in the *b* and *c* directions. Therefore, ν(C1H···O1) is involved in the intermolecular translation T_a and intermolecular rotations R_a, R_b, and R_c. Remaining ν(N2H···N1) are involved in T_b and R_a. All hydrogen-bond stretching modes between molecules are obtained in the range of approximately 70−150 cm^{-1}. The ν(N2H···N1) at 76.05 cm^{-1} (peak 3) is the lowest-frequency mode among all stretching vibrations of weak hydrogen bonds, including the infrared-inactive modes. The slow stretching vibration of the N2H···N1 bond like peak 3 gives the water molecule a chance to attack the HOMO or LUMO of nicotinamide, which causes the hydrogen bond to switch. Among the three different hydrogen bonds in the nicotinamide crystal, the N2H···N1 and C1H···O1 hydrogen bonds were detected as stretching vibrations in the present THz spectrum (see Table 1). The ν(N2H···O1) is forbidden (the intensity is zero) and was not observed in the experiment.

5. CONCLUSIONS

We studied the temperature dependence of the THz spectrum of nicotinamide. We observed that almost all peaks in the spectrum show a remarkable frequency shift with temperature, whereas the lowest-frequency peak (peak 1) exhibits a negligible shift with temperature. We examined the effect of volume expansion and anharmonic potential energy. It is confirmed that the vibrational mode of peak 1 does not show the feature of the anharmonic potential energy. The stationary feature of peak 1 with temperature is explained by combining two effects, those giving the opposite frequency shift to low frequency due to the volume expansion with increasing temperature and those to high frequency due to intermolecular or interatomic repulsions. On the other hand, the vibrational modes of peaks 3 and 4 are anharmonic due to dissociation of a weak hydrogen bond and show a remarkable peak shift with temperature. Nicotinamide dissolves in water by cooperatively combining two different vibration modes with and without hydrogen-bond stretching. This finding suggests that the peaks in the THz spectrum can be systematically assigned using temperature-dependent measurements. The calculated intensity in the present pairwise scheme of dispersion correction[34] must be improved with the consideration of many-body vdW interactions for more accurate and quantitative discussion.[12,45]

AUTHOR INFORMATION

Corresponding Author

*E-mail: masae@fris.tohoku.ac.jp.

ORCID

Masae Takahashi: 0000-0001-7717-6512

Notes

The authors declare no competing financial interest.

ACKNOWLEDGMENTS

The authors thank Dr. H. Ito and Dr. M. Kumagai for their valuable advice and Ms. Y. Kamata for her technical support. The authors acknowledge the Center for Computational Materials Science of IMR, Tohoku University.

REFERENCES

(1) Baxter, J. B.; Guglietta, G. W. Terahertz Spectroscopy. *Anal. Chem.* **2011**, *83*, 4342−4368.

(2) Ueno, Y.; Ajito, K. Analytical Terahertz Spectroscopy. *Anal. Sci.* **2008**, *24*, 185−192.

DOI: 10.1021/acs.jpca.6b11049
J. Phys. Chem. A 2017, 121, 2558−2564

(3) Plusquellic, D. F.; Siegrist, K.; Heilweil, E. J.; Esenturk, O. Applications of Terahertz Spectroscopy in Biosystems. *ChemPhysChem* **2007**, *8*, 2412−2431.
(4) Kim, J.; Kwon, O.-P.; Jazbinsek, M.; Park, Y. C.; Lee, Y. S. First-Principles Calculation of Terahertz Absorption with Dispersion Correction of 2,2′-Bithiophene as Model Compound. *J. Phys. Chem. C* **2015**, *119*, 12598−12607.
(5) Pratik, S. M.; Chakraborty, S.; Mandal, S.; Datta, A. Cooperativity in a New Role: Stabilization of the Ammonium Salts in the Solid State over Their H-Bonded Complexes in the Gas Phase. *J. Phys. Chem. C* **2015**, *119*, 926−933.
(6) Li, J.-W.; Liu, Y.-Y.; Xie, L.-H.; Shang, J.-Z.; Qian, Y.; Yi, M.-D.; Yu, T.; Huang, W. Revealing the Interactions between Pentagon−Octagon−Pentagon Defect Graphene and Organic Donor/Acceptor Molecules: a Theoretical Study. *Phys. Chem. Chem. Phys.* **2015**, *17*, 4919−4925.
(7) Juliano, T. R.; Korter, T. M. London Force Correction Disparity in the Modeling of Crystalline Asparagine and Glutamine. *J. Phys. Chem. A* **2014**, *118*, 12221−12228.
(8) Delaney, S. P.; Witko, E. M.; Smith, T. M.; Korter, T. M. Investigating Tautomeric Polymorphism in Crystalline Anthranilic Acid Using Terahertz Spectroscopy and Solid-State Density Functional Theory. *J. Phys. Chem. A* **2012**, *116*, 8051−8057.
(9) King, M. D.; Korter, T. M. Modified Corrections for London Forces in Solid-State Density Functional Theory Calculations of Structure and Lattice Dynamics of Molecular Crystals. *J. Phys. Chem. A* **2012**, *116*, 6927−6934.
(10) King, M. D.; Ouellette, W.; Korter, T. M. Noncovalent Interactions in Paired DNA Nucleobases Investigated by Terahertz Spectroscopy and Solid-State Density Functional Theory. *J. Phys. Chem. A* **2011**, *115*, 9467−9478.
(11) King, M. D.; Korter, T. M. Application of London-Type Dispersion Corrections in Solid-State Density Functional Theory for Predicting the Temperature-Dependence of Crystal Structures and Terahertz Spectra. *Cryst. Growth Des.* **2011**, *11*, 2006−2010.
(12) Reilly, A. M.; Tkatchenko, A. Role of Dispersion Interactions in the Polymorphism and Entropic Stabilization of the Aspirin Crystal. *Phys. Rev. Lett.* **2014**, *113*, 055701.
(13) Takahashi, M. Terahertz Vibrations and Hydrogen-Bonded Networks in Crystals. *Crystals* **2014**, *4*, 74−103.
(14) Takahashi, M.; Ishikawa, Y. Translational Vibrations between Chains of Hydrogen-Bonded Molecules in Solid-State Aspirin Form I. *Chem. Phys. Lett.* **2013**, *576*, 21−25.
(15) Takahashi, M.; Ishikawa, Y. Terahertz Vibrations of Crystalline α-D-Glucose and the Spectral Change in Mutual Transitions between the Anhydride and Monohydrate. *Chem. Phys. Lett.* **2015**, *642*, 29−34.
(16) Takahashi, M.; Ishikawa, Y.; Ito, H. The Dispersion Correction and Weak-Hydrogen-Bond Network in Low-Frequency Vibration of Solid-State Salicylic Acid. *Chem. Phys. Lett.* **2012**, *531*, 98−104.
(17) Takahashi, M.; Ishikawa, Y.; Nishizawa, J.-I.; Ito, H. Low-Frequency Vibrational Modes of Riboflavin and Related Compounds. *Chem. Phys. Lett.* **2005**, *401*, 475−482.
(18) Takahashi, M.; Kawazoe, Y.; Ishikawa, Y.; Ito, H. Interpretation of Temperature-Dependent Low Frequency Vibrational Spectrum of Solid-State Benzoic Acid Dimer. *Chem. Phys. Lett.* **2009**, *479*, 211−217.
(19) *The Vitamins Fundamental Aspects in Nutrition and Health*, 4th ed.; Combs, G. F., Jr., Ed.; Academic Press: London, U.K., 2012.
(20) Ito, A.; Shirakawa, H.; Takumi, N.; Minegishi, Y.; Ohashi, A.; Howlader, Z. H.; Ohsaki, Y.; Sato, T.; Goto, T.; Komai, M. Menaquinone-4 Enhances Testosterone Production in Rats and Testis-Derived Tumor Cells. *Lipids Health Dis.* **2011**, *10*, 158.
(21) Watanabe-Kamiyama, M.; Kamiyama, S.; Horiuchi, K.; Ohinata, K.; Shirakawa, H.; Furukawa, Y.; Komai, M. Antihypertensive Effect of Biotin in Stroke-Prone Spontaneously Hypertensive Rats. *Br. J. Nutr.* **2008**, *99*, 756−763.
(22) Yu, B.; Huang, Z.; Wang, X.-Y.; Zhao, G.-Z. Study on THz Spectra of Nicotinic Acid, Nicotinamide and Nicotine. *Spectrosc. Spectral Anal.* **2009**, *29*, 2334−2337.
(23) Veszprémi, T.; Takahashi, M.; Ogasawara, J.; Sakamoto, K.; Kira, M. An ab Initio MO Study of Structure and Reactivity of 4-Silatriafulvene. *J. Am. Chem. Soc.* **1998**, *120*, 2408−2414.
(24) Takahashi, M.; Veszprémi, T.; Hajgató, B.; Kira, M. Theoretical Study on Stereochemical Diversity in the Addition of Water to Disilene. *Organometallics* **2000**, *19*, 4660−4662.
(25) Veszprémi, T.; Takahashi, M.; Hajgató, B.; Kira, M. The Mechanism of 1,2-Addition of Disilene and Silene. 1. Water and Alcohol Addition. *J. Am. Chem. Soc.* **2001**, *123*, 6629−6638.
(26) Takahashi, M.; Veszprémi, T.; Kira, M. 1,2-Addition Reaction of Monosubstituted Disilenes: An ab Initio Study. *Organometallics* **2004**, *23*, 5768−5778.
(27) Wulf, A.; Fumino, K.; Ludwig, R. Spectroscopic Evidence for an Enhanced Anion−Cation Interaction from Hydrogen Bonding in Pure Imidazolium Ionic Liquids. *Angew. Chem., Int. Ed.* **2010**, *49*, 449−453.
(28) Fumino, K.; Wulf, A.; Ludwig, R. The Cation−Anion Interaction in Ionic Liquids Probed by Far-Infrared Spectroscopy. *Angew. Chem., Int. Ed.* **2008**, *47*, 3830−3834.
(29) Wulf, A.; Fumino, K.; Ludwig, R.; Taday, P. F. Combined THz, FIR and Raman Spectroscopy Studies of Imidazolium-Based Ionic Liquids Covering the Frequency Range 2−300 cm^{-1}. *ChemPhysChem* **2010**, *11*, 349−353.
(30) Clark, S. J.; Segall, M. D.; Pickard, C. J.; Hasnip, P. J.; Probert, M. J.; Refson, K.; Payne, M. C. First Principles Methods Using CASTEP. *Z. Kristallogr. - Cryst. Mater.* **2005**, *220*, 567−570.
(31) Perdew, J. P.; Burke, K.; Ernzerhof, M. Generalized Gradient Approximation Made Simple. *Phys. Rev. Lett.* **1996**, *77*, 3865−3868.
(32) Perdew, J. P.; Burke, K.; Ernzerhof, M. Generalized Gradient Approximation Made Simple. *Phys. Rev. Lett.* **1997**, *78*, 1396.
(33) Hakey, P. M.; Allis, D. G.; Hudson, M. R.; Ouellette, W.; Korter, T. M. Investigation of (1R,2S)-(−)-Ephedrine by Cryogenic Terahertz Spectroscopy and Solid-State Density Functional Theory. *ChemPhysChem* **2009**, *10*, 2434−2444.
(34) Tkatchenko, A.; Scheffler, M. Accurate Molecular Van Der Waals Interactions from Ground-State Electron Density and Free-Atom Reference Data. *Phys. Rev. Lett.* **2009**, *102*, 073005.
(35) Delaney, S. P.; Korter, T. M. Terahertz Spectroscopy and Computational Investigation of the Flufenamic Acid/Nicotinamide Cocrystal. *J. Phys. Chem. A* **2015**, *119*, 3269−3276.
(36) Miwa, Y.; Mizuno, T.; Tsuchida, K.; Taga, T.; Iwata, Y. Experimental Charge Density and Electrostatic Potential in Nicotinamide. *Acta Crystallogr., Sect. B: Struct. Sci.* **1999**, *55*, 78−84 (NICOAM01.cif, NICOAM05.cif).
(37) Grimme, S. Semiempirical GGA-Type Density Functional Constructed with a Long-Range Dispersion Correction. *J. Comput. Chem.* **2006**, *27*, 1787−1799.
(38) Iyengar, S. S. Dynamical Effects on Vibrational and Electronic Spectra of Hydroperoxyl Radical Water Clusters. *J. Chem. Phys.* **2005**, *123*, 084310.
(39) Li, X.; Moore, D. T.; Iyengar, S. S. Insights from First Principles Molecular Dynamics Studies toward Infrared Multiple-Photon and Single-Photon Action Spectroscopy: Case Study of the Proton-Bound Dimethyl Ether Dimer. *J. Chem. Phys.* **2008**, *128*, 184308.
(40) Iyengar, S. S. Computing Vibrational Properties in Hydrogen-Bonded Systems Using Quantum Wavepacket Ab Initio Molecular Dynamics. *Int. J. Quantum Chem.* **2009**, *109*, 3798−3810.
(41) Li, X.; Oomens, J.; Eyler, J. R.; Moore, D. T.; Iyengar, S. S. Isotope Dependent, Temperature Regulated, Energy Repatitioning in a Low-Barrier, Short-Strong Hydrogen Bonded Cluster. *J. Chem. Phys.* **2010**, *132*, 244301.
(42) Dietrick, S. M.; Pacheco, A. B.; Phatak, P.; Stevens, P. S.; Iyengar, S. S. Influence of Water on Anharmonicity, Stability, and Vibrational Energy Distribution on Hydrogen-Bonded Adducts in Atmospheric Reactions: Case Study of the OH + Isoprene Reaction Intermediate Using An Initio Molecular Dynamics. *J. Phys. Chem. A* **2012**, *116*, 399−414.
(43) Desiraju, G. R.; Steiner, T. *The Weak Hydrogen Bond: In Structural Chemistry and Biology*; Oxford University Press: Oxford, U.K., 1999.

DOI: 10.1021/acs.jpca.6b11049
J. Phys. Chem. A 2017, 121, 2558−2564

(44) Steiner, T. The Hydrogen Bond in the Solid State. *Angew. Chem., Int. Ed.* **2002**, *41*, 48−76.
(45) Marom, N.; DiStasio, R. A., Jr.; Atalla, V.; Levchenko, S.; Reilly, A. M.; Chelikowsky, J. R.; Leiserowitz, L.; Tkatchenko, A. Many-Body Dispersion Interactions in Molecular Crystal Polymorphism. *Angew. Chem., Int. Ed.* **2013**, *52*, 6629−6632.

DOI: 10.1021/acs.jpca.6b11049
J. Phys. Chem. A 2017, 121, 2558−2564